Deep Resources Engineering 2 (2025) 100209

Contents lists available at ScienceDirect

Deep Resources Engineering

journal homepage: www.keaipublishing.com/en/journals/deepre/

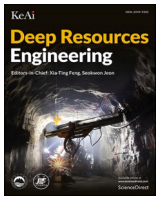

Full length article

Reservoir heterogeneity and its role in long-term CO_2 storage performance: A case study of Air Benakat formation

Romal Ramadhan [a,b,*], Muslim Abdurrahman [a,c,*], Agus Arsad [d], Anis Farhana Abdul Rahman [d], Veridaus Napitupulu [e], Witta Kartika Restu [f]

[a] Pusat Studi Pengembangan dan Peningkatan Produksi Minyak Bumi (PSP3MB), Universitas Islam Riau, Pekanbaru, Riau, Indonesia
[b] Department of Earth and Planetary Sciences, Jackson School of Geosciences, The University of Texas at Austin, TX, United States
[c] Department of Petroleum Engineering, Faculty of Engineering, Universitas Islam Riau, Pekanbaru, Riau, Indonesia
[d] UTM-MPRC Institute for Oil and Gas, Faculty of Chemical and Energy Engineering, Universiti Teknologi Malaysia, Johor Bahru, Malaysia
[e] Indogeo Social Enterprise, Jakarta, Indonesia
[f] Functional Molecule Chemistry Research Group, Badan Riset dan Inovasi Nasional (BRIN), Jakarta, Indonesia

ARTICLE INFO

Keywords:
Carbon capture and storage
Reservoir simulation
Role of heterogeneity
South Sumatra basin

ABSTRACT

Indonesia's strategy for attaining net-zero emissions by 2050 is contingent upon carbon capture and storage (CCS). The long-term CO_2 storage performance of Air Benakat formation in the South Sumatra Basin was assessed in this study, with a particular emphasis on the influence of reservoir heterogeneity. We compared the behavior of CO_2 (trapping mechanisms and migration) under homogeneous and heterogeneous conditions by utilizing reservoir modeling. Sequential Gaussian simulation (SGS) was implemented to represent spatial variability in porosity and permeability. Increased degrees of heterogeneity are quantified by Lorenz coefficients of permeability (*Lk*) of 0.0, 0.2, 0.4, and 0.6. The simulation results over a 1000-year period indicate that pressure accumulation during the 30-year injection phase is reduced, and pressure dissipation is enhanced post-injection as a consequence of increased heterogeneity. The distribution of permeability substantially impacts the trapping mechanisms for CO_2, including free-phase (supercritical), residual (trapped), and dissolved. Heterogeneous models exhibit greater long-term dissolution as a result of flow redistribution, whereas homogeneous models retain a larger amount of free-phase and trapped CO_2. Moreover, the consequences of heterogeneity are further illustrated by plume migration patterns. With the increase in *Lk* values, lateral migration becomes more asymmetric and fragmented, and the plume area expands by up to 23.4 % in comparison to the homogeneous case. Heterogeneity redirects CO_2 into additional strata without altering the maximal height, as evidenced by vertical plume analysis, with occupancy differences reaching up to 9.2 %. Overall, results highlight that ignoring heterogeneity leads to overestimations in CO_2 storage efficiency, particularly in trapped CO_2 capacity.

1. Introduction

The global urgency to address climate change and transition towards sustainable, low-carbon energy systems has reached an unprecedented level [1–3]. In response to this challenge, Indonesia, a country rich in natural resources and one of the world's largest carbon emitters, has set ambitious energy transition goals aimed at achieving a zero-carbon energy system by 2050 [4–6]. Reaching these targets requires active engagement across all sectors, especially within the energy and environmental domains, to reduce greenhouse gas emissions [7–9].

A key component of Indonesia's pathway toward a sustainable, carbon-neutral future is the reduction of carbon dioxide (CO_2) emissions through geological carbon capture and storage (CCS) technologies [10–12]. CCS is a globally recognized and widely implemented approach that involves capturing CO_2 emissions from industrial and power generation sources and storing them in deep geological formations to prevent their release into the atmosphere [13–15]. Among the various geological storage options, the injection of CO_2 into depleted hydrocarbon reservoirs is considered one of the most practical and effective strategies for emission reduction [16–19]. This is particularly relevant for Indonesia, given its vast hydrocarbon reserves [20–23].

This study focuses on evaluating CO_2 sequestration potential within a

* Corresponding authors at: Pusat Studi Pengembangan dan Peningkatan Produksi Minyak Bumi (PSP3MB), Universitas Islam Riau, Pekanbaru, Riau, Indonesia
E-mail addresses: romalramadhan@utexas.edu (R. Ramadhan), muslim@eng.uir.ac.id (M. Abdurrahman).

https://doi.org/10.1016/j.deepre.2025.100209
Received 20 June 2025; Received in revised form 26 July 2025; Accepted 24 August 2025
Available online 10 October 2025

specific geological setting: a depleted light oil reservoir located in South Sumatra Basin, as shown in Fig. 1. The basin, known for its geological complexity and substantial hydrocarbon resources, presents an excellent opportunity for implementing CCS initiatives [24–27].

Understanding the role of permeability heterogeneity is crucial, as it greatly affects the efficiency and viability of CCS projects [28–30] Variations in permeability significantly influence how CO_2 behaves during injection and long-term storage containment [31–33] To investigate this, we employed static reservoir simulation models designed to replicate homogeneous and heterogeneous reservoir conditions within South Sumatra Basin, specifically targeting Air Benakat formation.

Understanding how reservoir heterogeneity controls CO_2 storage processes is essential for designing effective injection strategies and ensuring long-term containment. Table 1 delineates the impact of several forms of reservoir physical heterogeneity on CO_2 storage. Variations in porosity and permeability, influenced by differing Lorenz coefficients, layered contrasts and overall heterogeneity, modify storage capacity, injectivity, plume migration patterns, and the equilibrium between dissolution and residual trapping [29,34,35]. Small-scale capillary pressure variability accelerates lateral plume movement and can triple capillary trapping [36,37]. Wettability heterogeneity enhances vertical plume penetration and dissolution while shifting trapping towards solubility [38]. In depleted gas reservoirs, increased permeability contrast and anisotropy enhance dispersion and channeling, with geological heterogeneity across lithologies broadening the range of volumetric displacement efficiency, albeit with only a modest effect on microscopic sweep.

2. Numerical model description

The middle Miocene Air Benakat Formation, located in the onshore South Sumatra Basin, is made up of interbedded volcaniclastic and clastic facies, including fine- to medium-grained sandstones, shales, siltstones, claystones, and coal streaks [24,27,42]. These types of rocks were deposited in fluviodeltaic to marginal marine environments [43]. Large pore volume for storage and high injectivity for effective CO_2 injection are provided by reservoir sands, which have typical porosities of about ~25 %, and permeabilities of up to ~1 D [44]. While structural compartmentalization by faulting defines distinct storage traps that make plume management and leakage monitoring easier, the Gumai shale and intraformational mudstones that lie on top act as regionally extensive cap and baffle seals [45]. Long-term seal integrity is confirmed by proven hydrocarbon containment in these same sandstones, and high-density storage is ensured by burial depths compatible with supercritical CO_2 conditions, making the Air-Benakat formation an ideal target for large-scale geological CCS.

The Air Benakat formation was selected as a representative site to evaluate the feasibility of CCS in Indonesia. Fig. 2 illustrates the relative permeability curves of Air Benakat formation, while Table 2 provides a detailed summary of the key reservoir properties used in our numerical models. To resolve both lateral plume migration and fine-scale vertical heterogeneity, we defined a 5×5 mi^2 ($\approx 8.05 \times 8.05$ km^2) domain and discretized it into a $100 \times 100 \times 60$ Cartesian grid (600,000 cells), yielding block sizes of ≈ 80.5 m $\times$ 80.5 m $\times$ 3.3 m, with the injection well set in the center of reservoir. The formation lies at a depth of 1300–1500 m [46–48]. It covers a thickness of 200 m, where the upper 10 layers (Sw ranges from 63 % to 97 %) were set to be the oil zone [46] and the remaining net thickness serves as the underlying aquifer. Predominantly composed of sandstone [42], the formation exhibits a porosity of 0.247, which provides favorable conditions for CO_2 injection and migration. The anisotropy ratio (kV/kH) was set to 0.1, following the common rule of thumb in layered clastic reservoirs that thin shale baffles typically reduce vertical permeability by an order of magnitude while still allowing some cross-bedding connectivity, and initial reservoir conditions correspond to a depleted pressure of 1278 psi ($\approx$ 8.8 MPa) and temperature of 150 °F ($\approx$ 66 °C). Due to the scarcity of field-scale data, the reservoir boundary is considered a closed, no-flow system.

To address spatial uncertainty in reservoir properties that are critical to CO_2 storage performance, we employed sequential Gaussian simulation (SGS) with a normal transform [49,50]. We generated an equiprobable realizations of porosity (ϕ) and multiple permeabilities (k), offering an uncertainty propagation depiction of heterogeneity within Air Benakat formation. These realizations provided the foundation for evaluating flow pathways, pressure distribution, and plume dispersion under different geological scenarios. To further characterize the reservoir's flow behavior, we conducted a linear regression analysis to quantify the empirical relationship between porosity and permeability. The spatial patterns derived from SGS, along with the observed porosity distribution, are illustrated in Fig. 3.

In this study, we used Lorenz coefficients (Lk) [51] to quantify and represent reservoir heterogeneity, as shown in Fig. 4. A Lorenz coefficient of 0.2 reflects moderate permeability variation, with values ranging from 100 to 500 millidarcies (mD). In contrast, a coefficient of 0.6 indicates a much higher degree of heterogeneity, with permeability values ranging from 10 to 2000 mD. This level of variation suggests that geological formation contains a wide distribution of both high- and low-permeability zones. We also compared the heterogeneous models with a homogeneous model (where it has 0.0 Lk) in the next sections. Detailed equations for Lk heterogeneity model is discussed in section S4.

In our study, Fig. 5 visually presents the permeability distribution for different Lorenz coefficients. It illustrates the variations in permeability corresponding to Lk values of 0.2, 0.4, and 0.6, effectively demonstrating how the reservoir's permeability heterogeneity changes under

Fig. 1. Location map of Air Benakat formation in South Sumatra Basin.

Table 1
Impact of reservoir physical heterogeneity on CO_2 storage dynamics.

Heterogeneity of reservoir properties	CO_2 storage behavior observed
Porosity & permeability	Rasheed et al. used numerical simulations with varying Lorenz coefficients to show that increasing heterogeneity reduces overall storage capacity and residual trapping while dissolution trapping dominates, that highly heterogeneous aquifers end injection at lower pressures with shorter injection-rate stability, and that low to medium heterogeneity combined with good porosity delivers the most favorable pressure behavior and injectivity [35]. Fang et al. showed that in randomly multilayered saline formations, permeability heterogeneity governs CO_2 plume mobility by driving it laterally along high-permeability layers with little vertical migration, and that this heterogeneity is the primary factor determining overall CO_2 dissolution efficiency [29]. Al-Khdheeawi et al. reported that CO_2 plumes achieve greater vertical migration in homogeneous reservoirs than in heterogeneous ones [31]. Gershenzon et al. examined how small-scale heterogeneity in deep saline aquifers affects CO_2 trapping and found that variations in capillary entry pressures among different materials enhance CO_2 immobilization in heterogeneous media. They concluded that capillary trapping in highly heterogeneous reservoirs far surpass that in more uniform ones [39]. Rezk and Ibrahim applied a field-scale compositional model of the Sleipner Utsira aquifer with varied Dykstra–Parsons coefficients and found that increasing geological heterogeneity only slightly changes structural trapping but substantially shifts storage toward solubility trapping at the expense of residual trapping by generating more and longer density fingers, while also promoting wider lateral plume spread and restricting upward migration [34]. Myshakin et al. used numerical simulations in geostatistically heterogeneous reservoir models across various lithologies and depositional environments to show that geological heterogeneity strongly influences volumetric displacement efficiency, widening its variability, while having only a modest impact on microscopic displacement efficiency, and that higher pressure, temperature, and injection rates tend to boost volumetric efficiency whereas greater permeability anisotropy reduces both efficiency metrics [40]. Mawa et al. used 2D and 3D stochastic models of depleted gas reservoirs to show that higher permeability heterogeneity (VDP) and larger vertical-to-horizontal permeability ratios boost CO_2 dispersion and channeling, while water saturation and gas solubility control the mixing zone size and Peclet number [41].
Capillary pressure	Jackson and Krevor investigated how small-scale capillary heterogeneities affect plume migration and showed that layering can boost lateral migration rates by up to 200 % [37]. Harris et al. investigated how variability in capillary pressure influences residual trapping and found that greater heterogeneity can boost capillary trapping by up to threefold [36].
Wettability	Al-Khdheeawi et al. found that wettability heterogeneity significantly increases vertical CO_2 plume migration, which enhances dissolution, and that it alters trapping behavior by reducing residual trapping while boosting solubility trapping, ultimately raising the volume of transportable CO_2 [38].

different scenarios. The permeability distributions at *Lk* values of 0.2, 0.4, and 0.6 [51–53] were each generated with an average permeability of 150 mD. For homogeneous case, the porosity and permeability were set to the average value as in Table 2.

The fluid model used in this study is based on the composition of

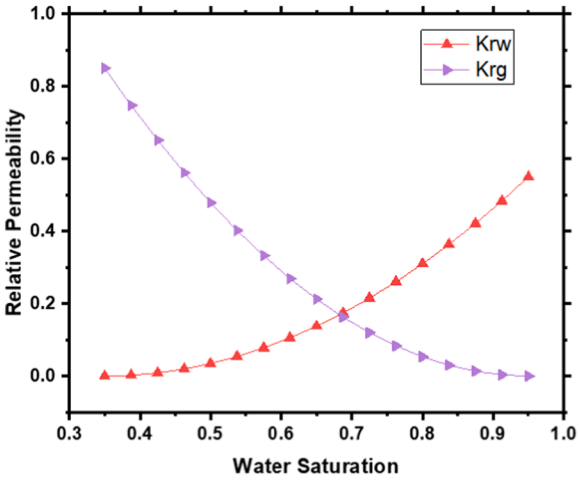

Fig. 2. Relative permeability curves of Air Benakat formation.

Table 2
Summary of reservoir properties.

Property	Value
Top depth (m)	1300
Grid dimension	100 × 100 × 60
Reservoir size (mile)	5 × 5
Thickness (m)	200
Rock type	Sandstone
Porosity (%)	24.7
kV/kH	0.1
Reservoir pressure (psi)	1278
Reservoir temperature (°F)	150
Sw (%)	63 – 97 %

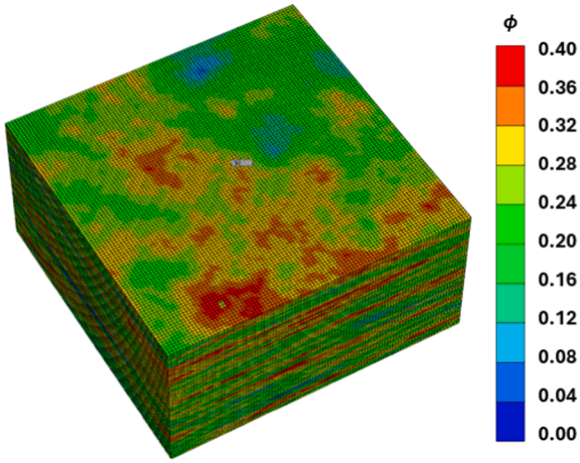

Fig. 3. Porosity distribution of Air Benakat formation.

light oil from Air Benakat formation, as presented in Fig. 6. We began by using WINPROP to characterize the reservoir fluid. Next, we imported the detailed fluid model into CMG-GEM for further simulation [8]. To model the CO_2 trapping mechanisms, we applied a generalized Peng-Robinson equation of state (EoS) [54] within CMG-GEM to predict and analyze phase behavior, solubility, and thermodynamic properties of CO_2 under subsurface temperature and pressure conditions during the injection phase, see Table 3. We used the Jossi, Stiel, and Thodos correlation to estimate fluid viscosity. For water properties, we calculated density using the Rowe and Chou correlation [55] and viscosity using the Kestin et al. correlation [56]. To account for gas dissolution in the

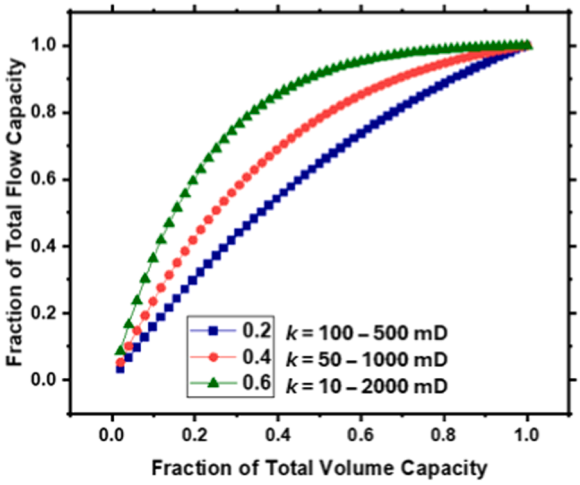

Fig. 4. Lorenz coefficient of the permeability distribution.

aqueous phase during injection and long-term migration, we applied Henry's law [57,58]. The governing equations used for the simulation is presented in section (S1) – (S3).

The injection rate was set to 1 Mtpa of CO_2 a period of 30 years, and we continued to run the simulation to 1000 years to see how plume migrates in the formation under different permeability heterogeneity scenarios. Note that geochemical reactions (e.g. mineral trapping) and geomechanical coupling were not included in this study.

3. Results and discussion

3.1. Pressure

Fig. 7 and Table 4 illustrate that all realizations demonstrate a fast increase in pressure during the 30-year CO_2 injection phase, after by a gradual decrease and stabilization over the next 970 years. Commencing with the initial diminished reservoir pressure of 1278 psi, the homogeneous model ($Lk = 0$) attains a maximum of around 1707 psi by the thirtieth year. The systematic introduction of permeability heterogeneity reduces the maximum values: examples with $Lk = 0.2$, 0.4, and 0.6 stabilize at roughly 1684 psi, 1665 psi, and 1644 psi, respectively. Increased permeability contrasts create preferential flow paths, reducing overall resistance and thus limiting pressure buildup for the same injection rate.

Once injection stops at year 30, pressure in the well region relaxes as fluids redistribute. All cases exhibit a 10–20 psi drop over the next 70 years. The more heterogeneous models ($Lk \geq 0.4$) show slightly faster decline, reflecting enhanced connectivity to lower-pressure regions. Pressures in all realizations approach a steady-state plateau beyond the year 100. The residual overpressure is highest in the homogeneous case,

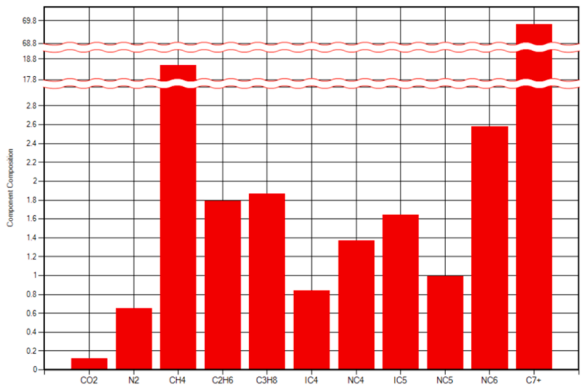

Fig. 6. Reservoir fluid composition [59].

Table 3
Compositional data calculated by Peng-Robinson EoS.

Component	Pc (atm)	Tc (K)	Acentric Factor	MW	Vc (l/mol)
CO_2	72.8	304.2	0.225	44.010	0.094
N_2	33.5	126.2	0.040	28.013	0.090
CH_4	45.4	190.6	0.008	16.043	0.099
C_2H_6	48.2	305.4	0.098	30.070	0.148
C_3H_8	41.9	369.8	0.152	44.097	0.203
IC_4	36.0	408.1	0.176	58.124	0.263
NC_4	37.5	425.2	0.193	58.124	0.255
IC_5	33.4	460.4	0.227	72.151	0.306
NC_5	33.3	469.6	0.251	72.151	0.304
NC_6	29.3	507.4	0.296	86.178	0.370
C_{7+}	25.3	663.8	0.401	142.730	0.543

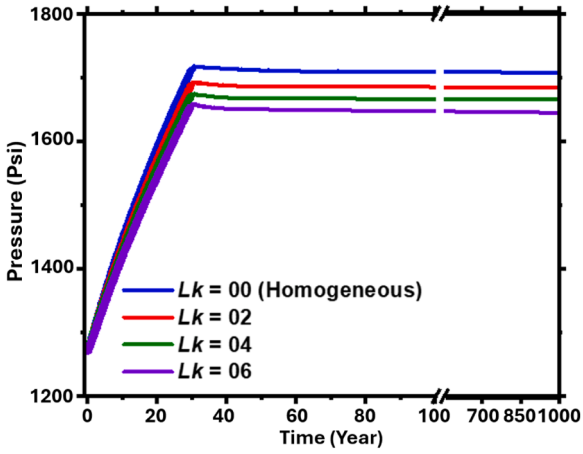

Fig. 7. Temporal pressure variation for homogeneous and heterogeneous permeability scenarios.

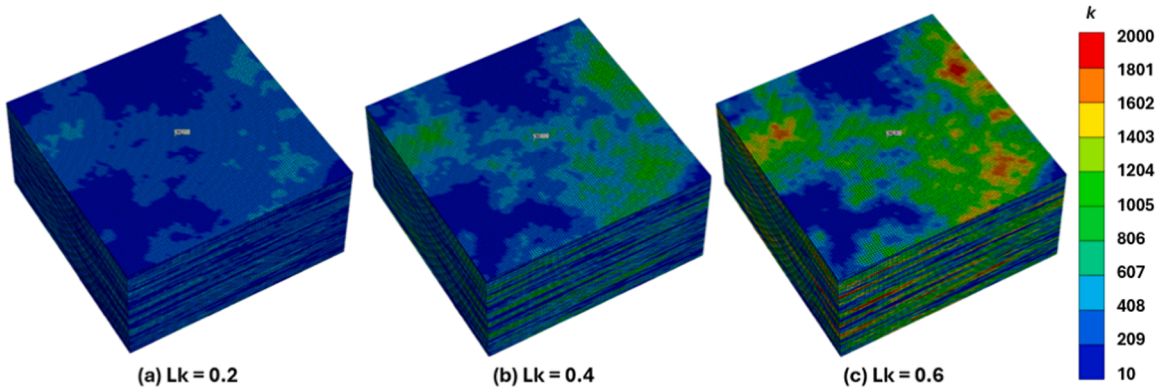

Fig. 5. Permeability distribution of Air Benakat formation: (a) $Lk = 0.2$; (b) $Lk = 0.4$; and (c) $Lk = 0.6$.

Table 4
Comparison of pressure drop due to permeability heterogeneity.

Case Comparison	Peak Pressure (psi)	ΔP (psi)	% Reduction
0.0 vs 0.2	1707 vs 1684	23	1.35 %
0.0 vs 0.4	1707 vs 1665	42	2.46 %
0.0 vs 0.6	1707 vs 1644	63	3.69 %

with the final well-block pressures remaining above the original 1278 psi by ~370 psi ($Lk = 0$) to ~330 psi ($Lk = 0.6$).

Rasheed et al. (2020) assert that permeability heterogeneity, as measured by the Lorenz coefficient (0.1 = low, 0.5 = medium, 0.78 = high), significantly influences pressure accumulation during CO_2 injection. After 30 years of uninterrupted injection, both low- and medium-heterogeneity scenarios attain comparable peak pressures (~479 bar), while the highly heterogeneous scenario demonstrates a markedly lower peak pressure [35].

3.2. CO_2 Trapping mechanisms

The evolution of the supercritical CO_2 over a 1,000-year period is depicted in Fig. 8 and Table 5 for four permeability heterogeneity scenarios. As the injection rate remains constant, all cases exhibit a nearly linear increase in free-phase CO_2 during the 30-year injection phase. The homogeneous model ($Lk = 0$) accumulates the most CO_2, with an estimated value of 5.88×10^{11} mol by year 30. Peak CO_2 accumulation experiences a modest decrease as the permeability contrast increases. The $Lk = 0.2$ case reaches a peak at $\sim 5.86 \times 10^{11}$ mol, whereas the most heterogeneous scenario ($Lk = 0.6$) only reaches $\sim 5.83 \times 10^{11}$ mol. This initial divergence is indicative of the more efficient dissolution of CO_2 into adjacent low-k regions and the enhanced distribution of CO_2 into high-permeability pathways under heterogeneous conditions.

As the system transitions from forced injection to natural pressure equilibration and dissolution trapping, the free-phase CO_2 accumulation begins to decrease upon shut-in at year 30. The CO_2 accumulation of the homogeneous model decreases by $\sim 0.21 \times 10^{11}$ mol from year 30 to 1000, from $\sim 5.88 \times 10^{11}$ to $\sim 5.67 \times 10^{11}$ mol. The declines in heterogeneous cases are marginally more pronounced: $Lk = 0.2$ decreases from $\sim 5.86 \times 10^{11}$ to $\sim 5.63 \times 10^{11}$ mol, $Lk = 0.4$ from $\sim 5.86 \times 10^{11}$ to $\sim 5.59 \times 10^{11}$ mol, and $Lk = 0.6$ from $\sim 5.83 \times 10^{11}$ to $\sim 5.55 \times 10^{11}$ mol.

The long-term free-phase CO_2 retention is still influenced by even moderate permeability contrasts, as evidenced by the ~1.7 percent variance between the homogeneous and most heterogeneous models. Ignoring heterogeneity in reservoir-scale assessments can result in overestimates of free-phase storage capacity, despite the fact that the absolute differences are still modest—on the order of 1–2 percent by year 1000.

Table 5
Comparison of free-phase CO_2 accumulation due to permeability heterogeneity.

Lk	CO_2 accumulation ($\times 10^{11}$ mol)			% Decrease
	Year 30	Year 1000	Drop	
0.0	5.88	5.67	0.21	3.57 %
0.2	5.86	5.63	0.23	3.93 %
0.4	5.86	5.59	0.27	4.61 %
0.6	5.83	5.55	0.28	4.80 %

Fig. 9 and Table 6 illustrate the temporal progression of entrapped CO_2 across the four cases of permeability heterogeneity. The advancing buoyant plume displaces saline and leaves behind residual saturations, resulting in the rapid accumulation of confined CO_2 during the 30-year injection phase. The homogeneous model ($Lk = 0$) achieves the highest confined volume, which reaches a peak of $\sim 1.22 \times 10^{11}$ mol by year ~80, whereas heterogeneity systematically diminishes this peak. The $Lk = 0.2$ case has a value of $\sim 1.05 \times 10^{11}$ mol, $Lk = 0.4$ is $\sim 0.96 \times 10^{11}$ mol, and $Lk = 0.6$ is only $\sim 0.86 \times 10^{11}$ mol. This trend is the result of the fact that high-permeability channels in heterogeneous models concentrate flow and bypass low-permeability regions, where residual entrapment is most effective.

Diffusional dissolution becomes the predominant process from the year 100–1000, resulting in the flattening of the confined CO_2 curves as concentration gradients decrease. The homogeneous model stabilizes at $\sim 1.09 \times 10^{11}$ mol of sequestered CO_2 by the end of the millennium, while the $Lk = 0.2$, 0.4, and 0.6 cases resolve at ~0.86, ~0.72, and $\sim 0.56 \times 10^{11}$ mol, respectively. The permeability heterogeneity can significantly reduce the long-term efficacy of trapped CO_2, as evidenced by the increasing spread, up to $\sim 0.53 \times 10^{11}$ mol (~49 %) between the homogeneous ($Lk = 0.0$) and most heterogeneous of the cases ($Lk = 0.6$). Therefore, disregarding the heterogeneity may result in overestimations of the amount of CO_2 immobilized by capillary forces.

Fig. 10 and Table 7 show the evolution of dissolved CO_2 over a 1000-year period. Dissolved CO_2 accumulates swiftly during the 30-year injection phase as supercritical CO_2 interacts with saline. The heterogeneous cases achieve slightly lower values, ~0.52, ~0.51, and $\sim 0.50 \times 10^{11}$ mol for $Lk = 0.2$, 0.4, and 0.6, respectively, while the homogeneous model ($Lk = 0$) reaches $\sim 0.54 \times 10^{11}$ mol by year 30.

The disparities in dissolved CO_2 between the permeability scenarios are most apparent at year 1000. The most heterogeneous case ($Lk = 0.6$) achieves the highest value, $\sim 0.86 \times 10^{11}$ mol. Followed by $Lk = 0.4$ at $\sim 0.83 \times 10^{11}$ mol, Lk = 0.2 at $\sim 0.79 \times 10^{11}$ mol, and the homogeneous case ($Lk = 0.0$) at $\sim 0.77 \times 10^{11}$ mol.

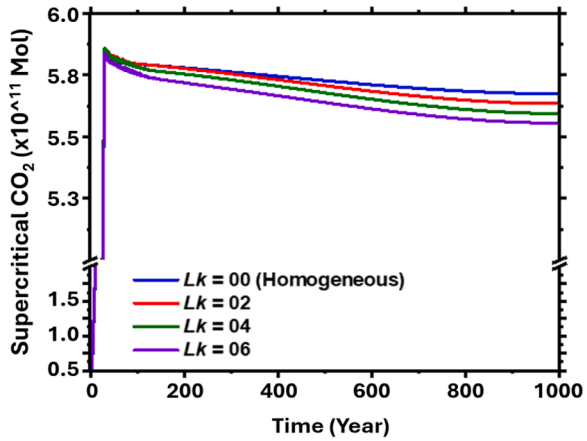

Fig. 8. Temporal dynamics of supercritical CO_2 for homogeneous and heterogeneous permeability scenarios.

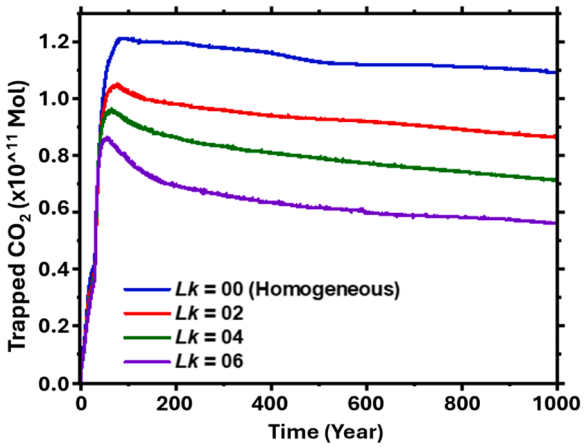

Fig. 9. Temporal dynamics of trapped CO_2 for homogeneous and heterogeneous permeability scenarios.

Table 6
Comparison of trapped CO_2 accumulation due to permeability heterogeneity.

Lk	CO_2 accumulation ($\times 10^{11}$ mol)			% Decrease
	Year 80	Year 1000	Drop	
0.0	1.22	1.09	0.13	10.70 %
0.2	1.05	0.86	0.19	18.10 %
0.4	0.96	0.72	0.24	25.00 %
0.6	0.86	0.56	0.3	34.90 %

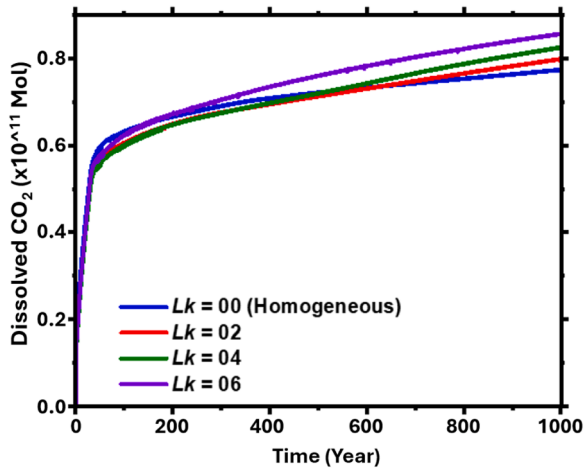

Fig. 10. Temporal dynamics of dissolved CO_2 for homogeneous and heterogeneous permeability scenarios.

Table 7
Comparison of dissolved CO_2 accumulation due to permeability heterogeneity.

Lk	CO_2 accumulation ($\times 10^{11}$ mol)			% Increase
	Year 30	Year 1000	Rise	
0.0	0.54	0.77	0.23	42.60 %
0.2	0.52	0.79	0.27	51.90 %
0.4	0.51	0.83	0.32	62.70 %
0.6	0.50	0.86	0.36	72.00 %

The more heterogeneous systems progressively surpass the homogeneous case in dissolved CO_2 mass, as they benefit from enhanced fluid mixing and prolonged convective circulation, despite the homogeneous model initially leading during the injection phase. The heterogeneity of the $Lk = 0.6$ and $Lk = 0.0$ scenarios results in an increase of ~12 % by the year 1000, with a difference of $\sim 0.09 \times 10^{11}$ mol.

3.3. Plume migration

3.3.1. Lateral migration

The lateral migration of the CO_2 plume is compared in Fig. 11 for four degrees of permeability heterogeneity at 30, 100, 500, and 1000 years. The plume remains essentially circular throughout the simulation for the homogeneous case ($Lk = 0.0$; Fig. 11a). At 30 years (the end of injection), it displays a smooth, radially symmetric front. The radius is marginally reduced by minor capillary-driven polishing over a period of 100 years, while circularity is maintained. Diffusion and capillary forces induce only a slight contraction, even at 500 and 1000 years.

At 30 years, the plume edge remains nearly uniform, with only incipient expansion into higher-permeability zones, for mild heterogeneity ($Lk = 0.2$; Fig. 11b). This elongation becomes more pronounced after 100 years, as the plume advances preferentially in one direction while the opposite flank delays. The homogeneous case is surpassed by the lateral spread along the more permeable pathway at 500 years. From the end of the injection, asymmetry is the predominant characteristic at moderate heterogeneity ($Lk = 0.4$; Fig. 11c). The 30-year plume has already been extended along high-permeability corridors, and its leading edge swiftly advances to form a prominent lobe over the next 70 years, while the trailing edge remains virtually stationary. The plume is highly distorted with considerable variability in thickness by 1000 years.

Lateral migration is uneven and rapid in the presence of strong heterogeneity ($Lk = 0.6$; Fig. 11d). The centroid of the plume has a significant shift toward the most permeable pathways even at the year 30, and by the year of 100, the leading front has advanced nearly twice as far as the opposite edge. The injected CO_2 front breaks into multiple isolated pockets linked by narrow channels by year 500, and by year 1000 it's nearly completely scattered into tiny, disconnected fragments.

Fig. 12a illustrates that a narrow band of excess plume area of ~875 cells (8.8 %) develop on the high-permeability side by 30 years when $Lk = 0.2$. During the subsequent 70 years, this band contracts to ~674 cells (6.7 %) at 100 years, and then widens again to ~844 cells (8.4 %) at 500 years. The added footprint reaches 669 cells (6.7 %) after 1000 years, suggesting a persistent but fluctuating deviation from the homogeneous case.

Two broad lobes of excess emerge immediately with moderate heterogeneity ($Lk = 0.4$; Fig. 12b). The plume experiences a ~1246 cell increase (12.5 %) at the 30-year mark, and this surplus remains essentially unchanged at the 100-year mark (~1248 cells; 12.6 %). The additional area increases to ~1522 cells (15.2 %) as the lobes extend into slender, finger-like protrusions over the course of 500 years. The lobes, which retain a distinctly oblate imprint, slightly retract to ~1259 cells (12.6 %) at 1000 years.

The plume's excess area is both the largest and most complex when the highest heterogeneity is present ($Lk = 0.6$; Fig. 12c). By the year of 30, a broad crescent of ~1673 cells (16.7 %) is visible, which expands into pronounced lobes of ~1909 cells (19.1 %) by the year of 100. At 500 years, the lobes of the CO_2 plume break up into many thin, elongated strands, with a maximum of ~2339 cells (23.4 %). The excess area decreases to ~1789 cells (17.9 %) over a period of 1000 years, but the footprint remains highly irregular and compartmentalized.

Prior research in 2015, by Gershenzon et al. shown that clusters of open-framework gravel within small-scale fluvial architecture create laterally interconnected "thief-zones" that direct injected CO_2 onto branching paths, significantly augmenting the plume's lateral migration via high-permeability channels [60]. Another study by Sohal et al. (2021) described that permeability contrasts and facies architecture create preferential pathways that enhance lateral plume spread while also producing additional trapping in lower-permeability zones [61].

3.3.2. Vertical migration

The CO_2 plume's vertical extent remains essentially similar across all heterogeneity levels at 30 years. However, subtle distinctions are observed when comparing each case to the homogeneous baseline ($Lk = 0.0$). The overall shape and apex height of the plume remain approximately equal for $Lk = 0.2$, as illustrated in Fig. 13 (saturation cross-sections). However, the finer-scale fingers enter high-permeability layers slightly deeper. This is quantified in Fig. 14a: A modest but detectable shift in vertical migration paths is indicated by the fact that ~205 (3.4 %) grid cells differ between the $Lk = 0.0$ and $Lk = 0.2$ occupancy maps, out of 6000.

Fig. 13 displays more prominent vertical lobes and undulations along permeability lines, despite moderate heterogeneity ($Lk = 0.4$). Fig. 14b captures ~362 distinct cells (6.0 % of 6000), demonstrating that a greater proportion of CO_2 is directed to preferential layers as a result of increased heterogeneity, despite the fact that the maximal plume height remains consistent. The plume cross-section in Fig. 13 indicates the most irregular base and side-wall incursion when heterogeneity is strong ($Lk = 0.6$). In year 30, Fig. 14c confirms that up to nearly one-tenth of the vertical plume footprint transitions into new strata as *Lk* increases, with

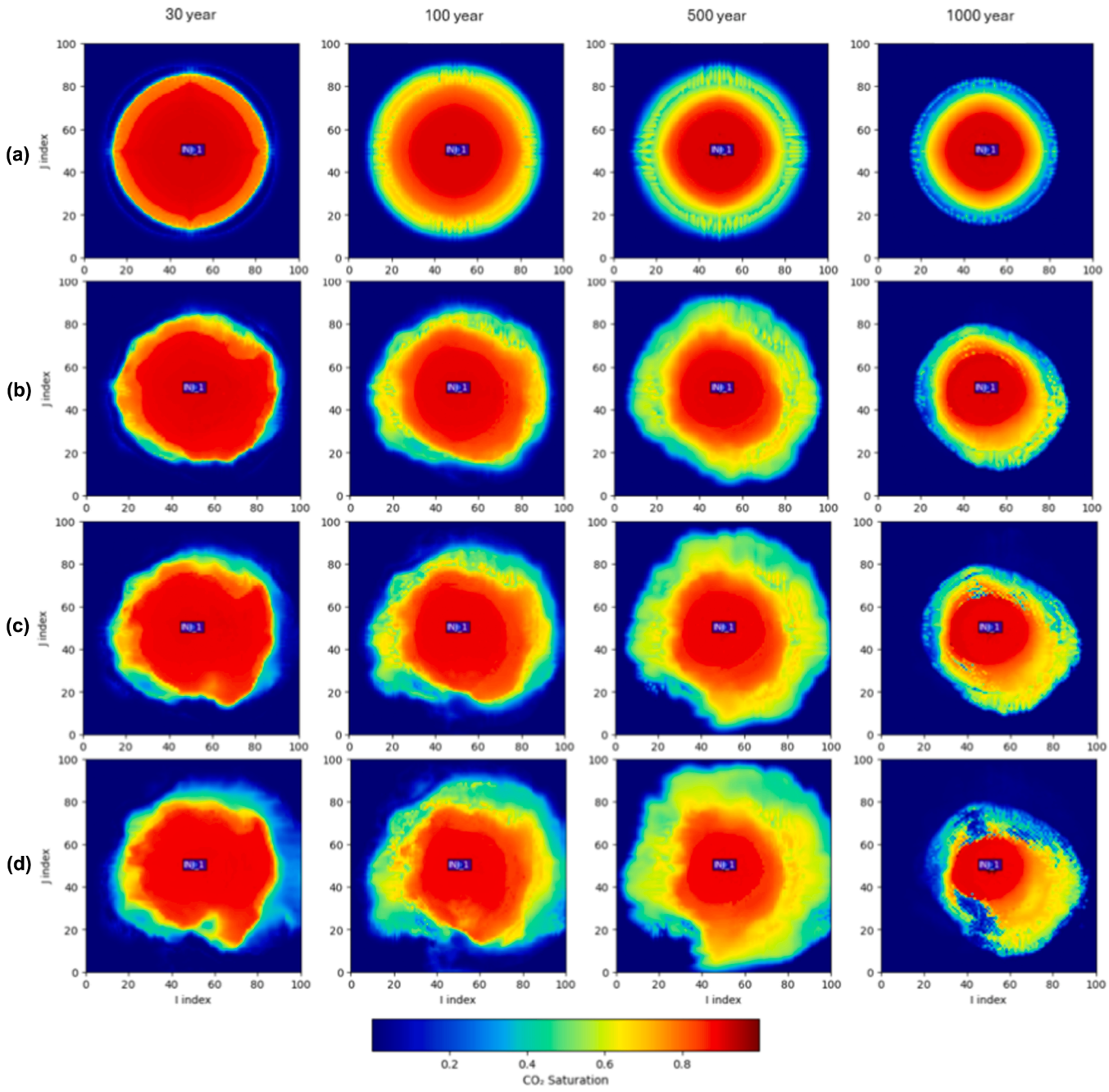

Fig. 11. Temporal evolution of CO_2 plume lateral migration at 30, 100, 500, and 1000 years for varying permeability heterogeneity: (a) *Lk*=0.0; (b) *Lk*=0.2; (c) *Lk*=0.4; and (d) *Lk*=0.6.

~550 distinct cells (9.2 %), the comparison of homogeneous against each case of heterogeneous is summarized in Table 8.

3.4. Implications for CCS site selection and risk assessment

Our findings indicate that the selection of CCS sites and risk assessments must explicitly consider reservoir heterogeneity, as characterized by porosity and permeability distributions determined from well data and SGS realizations. Dynamic 3D models derived from this data produce more conservative estimates of storage capacity by accounting for diminished trapped CO_2 and improved dissolution. They assist in planning injection pressure to manage compartmentalization and prevent overpressure, while also defining an expanded Area of Review (AoR) for full-scale injection. This is crucial as asymmetric, fragmented plume footprints in heterogeneous systems can extend further than those in homogeneous counterparts. Consequently, these models facilitate optimal placement of monitoring wells along predicted high-permeability corridors and inform the sizing of post-injection seismic surveys to encompass the actual dispersion of the CO_2 plume.

This heterogeneity-induced plume behavior has two significant practical implications. Initially, monitoring must be more spatially comprehensive and focused: asymmetric, fragmented CO_2 footprints necessitate the deployment of pressure and saturation sensors along anticipated high-permeability corridors and up-dip extents, rather than in a simplistic, symmetric arrangement, and the monitoring network should be expanded to encompass the enlarged AoR identified by SGS-based plume realizations. Secondly, storage-capacity estimation should progress beyond singular, uniform forecasts: by executing ensembles of realizations, each characterized by unique porosity and

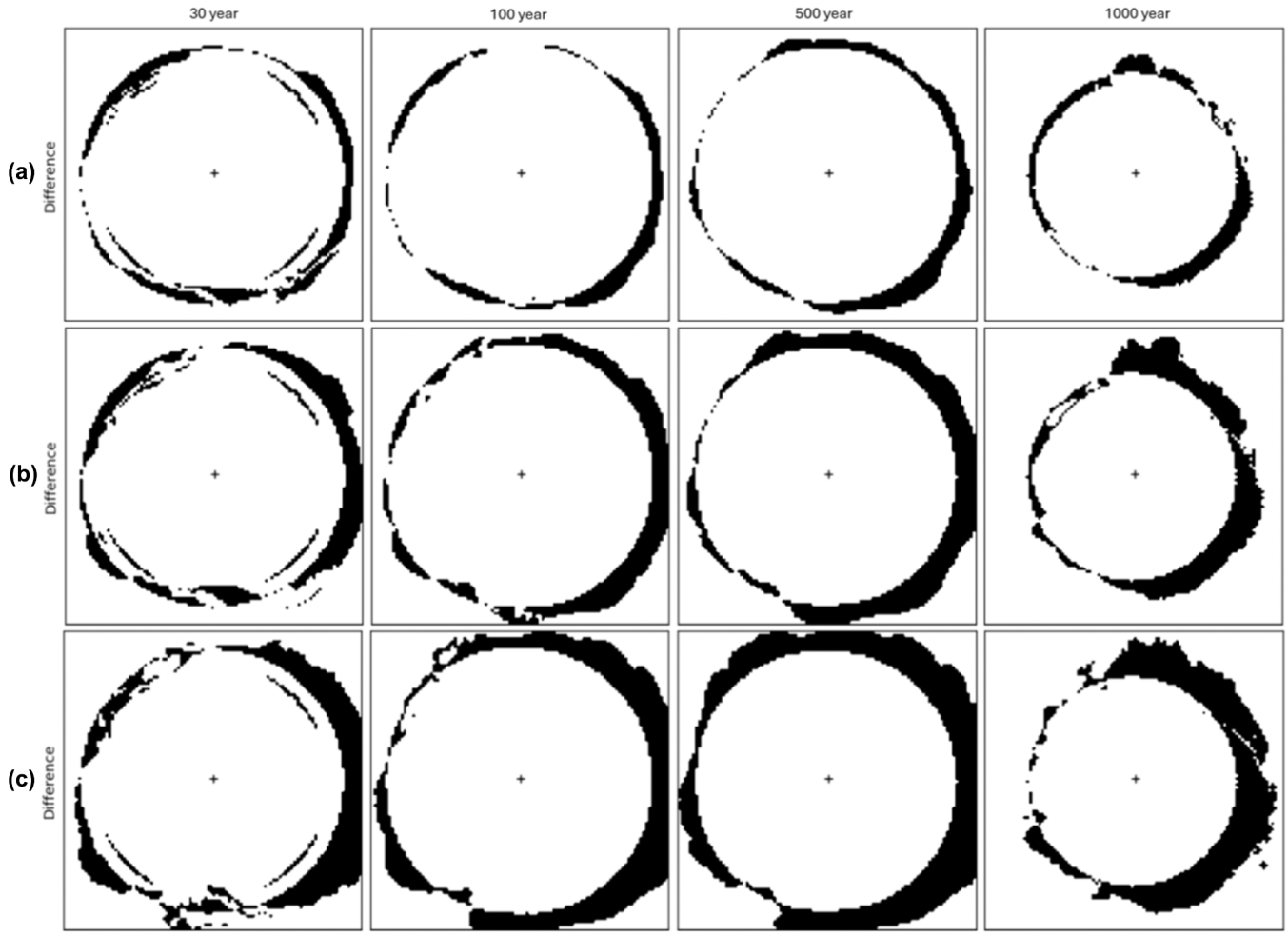

Fig. 12. Spatial difference maps of the CO_2 plume footprint relative to the homogeneous case ($Lk = 0.0$) at 30, 100, 500, and 1000 years for heterogeneity levels: (a) $Lk = 0.2$; (b) $Lk = 0.4$; and (c) $Lk = 0.6$.

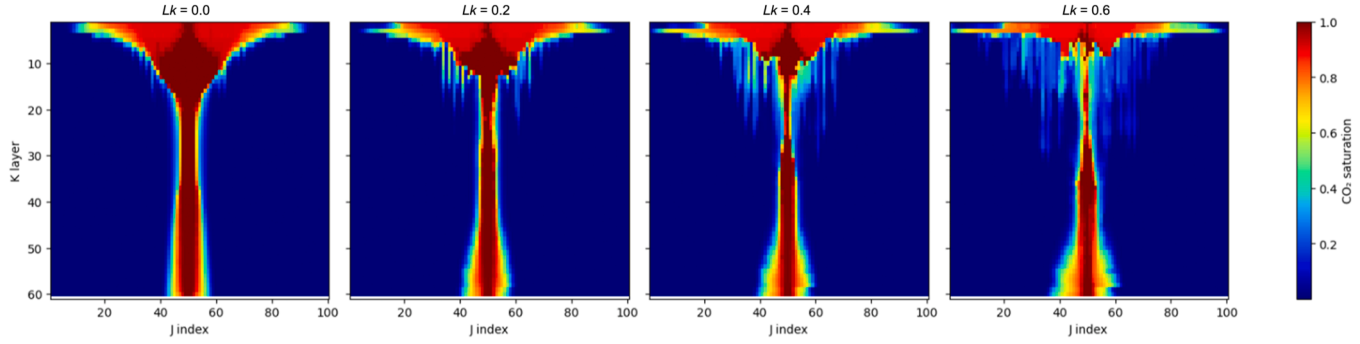

Fig. 13. Vertical cross-sections of CO_2 saturation in the J–K plane for increasing permeability heterogeneity at year-30.

permeability fields, operators can produce probabilistic CO_2 retention curves (free-phase, trapped, and dissolved), encompassing the spectrum of probable capacities and guaranteeing conservative designs, given that models neglecting heterogeneity generally overestimate trapped CO_2 and underestimate long-term dissolution.

4. Conclusion

(1) In comparison to the homogeneous scenario (1707 psi), the introduction of permeability heterogeneity results in a decrease in peak pressure of 23 psi (1.35 %) for $Lk = 0.2$, 42 psi (2.46 %)

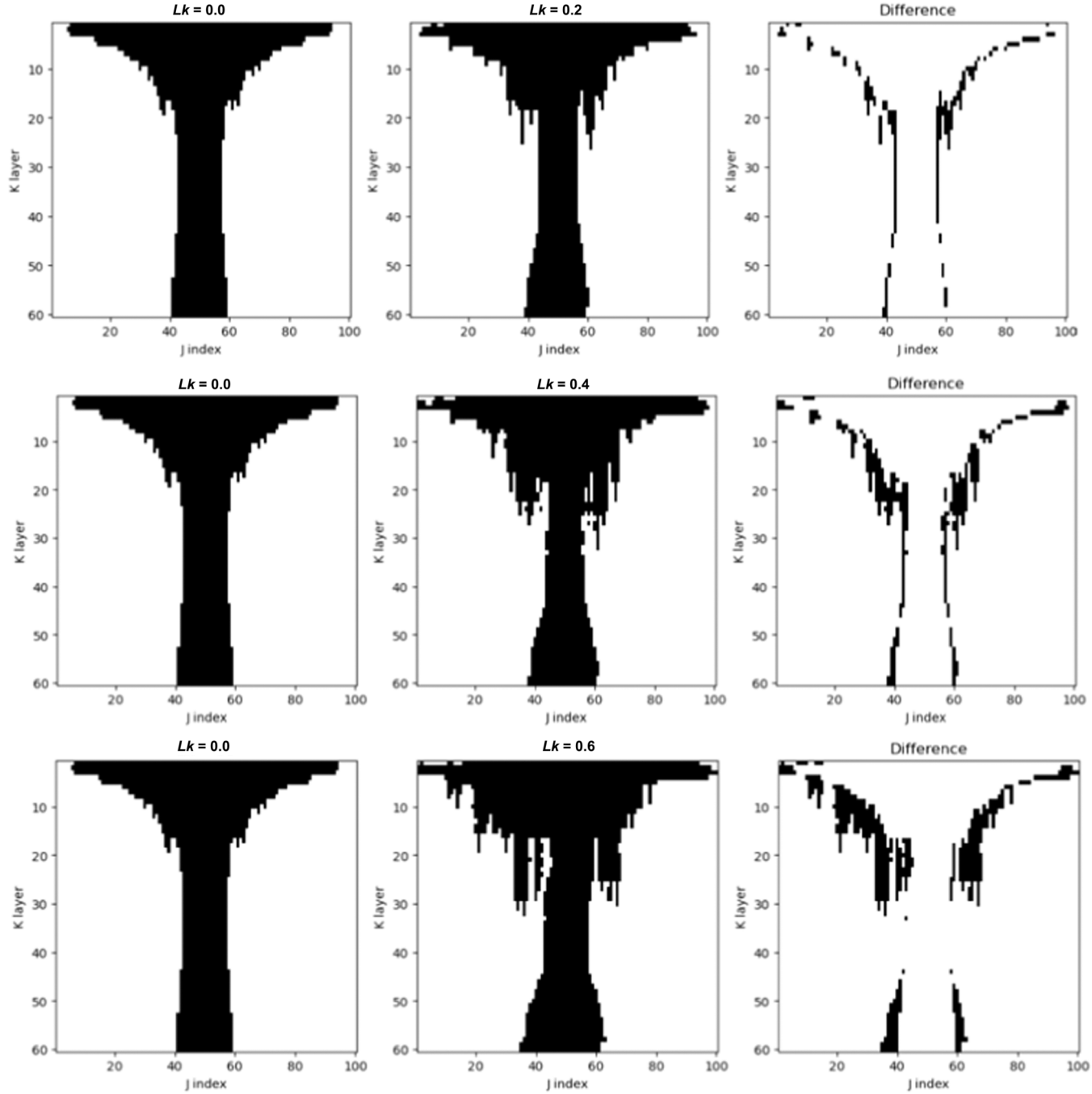

Fig. 14. Binary occupancy maps and their differences relative to the homogeneous case in the J–K plane, shown for each heterogeneity at year 30.

Table 8
Comparison for vertical CO_2 migration.

Comparison	Differing Cells	Percentage
Lk 0.0 vs 0.2	205	3.40 %
Lk 0.0 vs 0.4	362	6.00 %
Lk 0.0 vs 0.6	550	9.20 %

for $Lk = 0.4$, and 63 psi (3.69 %) for $Lk = 0.6$. This trend indicates that greater heterogeneity progressively restricts pressure buildup during injection.

(2) Permeability heterogeneity leads to a gradual transition of CO_2 from free and trapped phases into the dissolved phase. An increase in *Lk* from 0.0 to 0.6 results in a reduction of free-phase accumulation at year 1000 from 3.57 % to 4.80 % and trapped accumulation from 10.7 % to 34.9 %, while dissolved CO_2 increases from 42.6 % to 72.0 %.

(3) As permeability heterogeneity intensified, the spatial deviation from the uniform baseline significantly enlarged. The quantity of distinct cells increases from ~205 (3.4 %) at $Lk = 0.2$ to ~550 (9.2 %) at $Lk = 0.6$, indicating that greater heterogeneity results in significantly enhanced model variety.

CRediT authorship contribution statement

Romal Ramadhan: Writing – original draft, Visualization, Software, Methodology, Investigation, Formal analysis, Data curation, Conceptualization. **Muslim Abdurrahman:** Writing – review & editing,

Validation, Supervision, Methodology. **Agus Arsad:** Writing – review & editing, Validation, Supervision. **Anis Farhana Abdul Rahman:** Writing – review & editing, Validation, Supervision. **Veridaus Napitupulu:** Validation, Data curation. **Witta Kartika Restu:** Writing – review & editing, Validation, Supervision.

Declaration of Competing Interest

The authors declare that they have no known competing financial interests or personal relationships that could have appeared to influence the work reported in this paper.

Acknowledgment

For the provision of the CMG simulator licenses, we are grateful to Computer Modeling Group Ltd. (Canada). The authors gratefully acknowledge the financial support from Universitas Islam Riau (UIR) through the research funding contract No. 1218/Kontrak/P-P-UGB/DPPM-UIR/11-2024. This support has been essential in enabling the completion of this study.

Appendix A. Supporting information

Supplementary data associated with this article can be found in the online version at doi:10.1016/j.deepre.2025.100209.

References

[1] M.R. Sule, W.G.A. Kadir, T. Matsuoka, et al., Gundih CCS pilot project: Current status of the first carbon capture and storage project in south and Southeast Asia regions (no. Jcm), SSRN Electron. J. (2020), https://doi.org/10.2139/ssrn.3366415.

[2] P. Fragkos, H.L. van Soest, R. Schaeffer, et al., Energy system transitions and low-carbon pathways in Australia, Brazil, Canada, China, EU-28, India, Indonesia, Japan, Republic of Korea, russia and the United States, Energy 216 (2021), https://doi.org/10.1016/j.energy.2020.119385.

[3] M.T. Sambodo, C.I. Yuliana, S. Hidayat, et al., Breaking barriers to low-carbon development in Indonesia: Deployment of renewable energy, Heliyon 8 (4) (2022) e09304, https://doi.org/10.1016/j.heliyon.2022.e09304.

[4] R. Ramadhan, M.T. Mon, S. Tangparitkul, et al., Carbon capture, utilization, and storage in Indonesia: An update on storage capacity, current status, economic viability, and policy, Energy Geosci. 5 (4) (2024) 100335, https://doi.org/10.1016/j.engeos.2024.100335.

[5] A. Rahman, R. Richards, P. Dargusch, et al., Pathways to reduce Indonesia's dependence on oil and achieve longer-term decarbonization, no. February 2022, Renew. Energy 202 (2023) 1305–1323, https://doi.org/10.1016/j.renene.2022.11.051.

[6] B.T.H. Marbun, D.E. Prasetyo, H. Prabowo, et al., Well integrity evaluation prior to converting a conventional gas well to CO_2 injector well – gundih CCS pilot project in Indonesia (phase 1), Int. J. Greenh. Gas. Control 88 (2019) 447–459, https://doi.org/10.1016/j.ijggc.2019.06.006.

[7] M.T. Mon, R. Tangsuchat, W. Yamaka, CCUS technology and carbon emissions: Evidence from the United States, Energies 17 (2024) 1.

[8] R. Ramadhan, K. Promneewat, V. Thanasaksukthawee, et al., Geomechanics contribution to CO_2 storage containment and trapping mechanisms in tight sandstone complexes: A case study on mae moh basin, Sci. Total Environ. 928 (2024) 172326, https://doi.org/10.1016/j.scitotenv.2024.172326.

[9] H. Chen, H.Z. Yu, B. Zhou, et al., Storage mechanism and dynamic characteristics of CO_2 dissolution in saline aquifers, Energy Fuels 37 (5) (2023) 3875–3885, https://doi.org/10.1021/acs.energyfuels.2c03987.

[10] A.N. Rakhiemah, Y. Xu, Economic viability of full-chain CCUS-EOR in Indonesia, no. November 2021, Resour. Conserv. Recycl 179 (2021) 106069, https://doi.org/10.1016/j.resconrec.2021.106069.

[11] D. Adisaputro, B. Saputra, Carbon capture and storage and carbon capture and utilization: What do they offer to Indonesia, no. March 2017, Front. Energy Res. 5 (2017) 2012–2015, https://doi.org/10.3389/fenrg.2017.00006.

[12] P.A. Aziz, T. Marhaendrajana, B.E.B. Nurhandoko, et al., Time-Dependent CO_2-Brine-Rock interaction effect on sand onset prediction: A case study of Dolomite-Rich sandstone in air benakat formation, south sumatra, Indonesia, ACS Omega (2025), https://doi.org/10.1021/acsomega.4c09499.

[13] J.G. Maas, N. Springer, A. Hebing, et al., Viscous fingering in CCS - a general criterion for viscous fingering in porous media, no. September 2023, Int. J. Greenh. Gas. Control 132 (2024), https://doi.org/10.1016/j.ijggc.2024.104074.

[14] H.C. Lau, Decarbonization of ASEAN's power sector: A holistic approach, Energy Rep. 9 (2023) 676–702, https://doi.org/10.1016/j.egyr.2022.11.209.

[15] N. Kumar, A. Verma, T. Ahmad, et al., Carbon capture and sequestration technology for environmental remediation: A CO_2 utilization approach through EOR, Geoenergy Sci. Eng. 234 (2024) 212619, https://doi.org/10.1016/j.geoen.2023.212619.

[16] S. Jitmahantakul, P. Chenrai, T. Chaianansutcharit, et al., Dynamic estimates of pressure and CO_2-storage capacity in carbonate reservoirs in a depleted gas field, northeastern Thailand (no. April), Case Stud. Chem. Environ. Eng. 8 (2023) 100422, https://doi.org/10.1016/j.cscee.2023.100422.

[17] P.A. Eigbe, O.O. Ajayi, O.T. Olakoyejo, et al., A general review of CO_2 sequestration in underground geological formations and assessment of depleted hydrocarbon reservoirs in the Niger delta, Appl. Energy 350 (2023) 121723, https://doi.org/10.1016/j.apenergy.2023.121723.

[18] X.L. Liu, H. Chen, Y. Li, et al., Oil production characteristics and CO_2 storage mechanisms of CO_2 flooding in ultra-low permeability sandstone oil reservoirs, Pet. Explor. Dev. 52 (1) (2025) 196–207, https://doi.org/10.1016/S1876-3804(25)60014-0.

[19] R. Ramadhan, C. Tapanya, T. Akamine, et al., CO_2 trapping dynamics in tight sandstone: Insights into trapping mechanisms in mae Moh's reservoir (no. September), J. Environ. Manag. 370 (2024) 122442, https://doi.org/10.1016/j.jenvman.2024.122442.

[20] H.K. Bokka, H.C. Lau, Decarbonizing Borneo's power and industry sectors by carbon capture and storage, no. September 2022, Geoenergy Sci. Eng. 226 (2023) 211796, https://doi.org/10.1016/j.geoen.2023.211796.

[21] K. Zhang, H.C. Lau, Regional opportunities for CO_2 capture and storage in Southeast Asia (no. February), Int. J. Greenh. Gas. Control 116 (2022) 103628, https://doi.org/10.1016/j.ijggc.2022.103628.

[22] H.C. Lau, The contribution of carbon capture and storage to the decarbonization of Coal-Fired power plants in selected asian countries, Energy Fuels (2023), https://doi.org/10.1021/acs.energyfuels.3c02648.

[23] H.C. Lau, Decarbonization roadmaps for ASEAN and their implications, Energy Rep. 8 (2022) 6000–6022, https://doi.org/10.1016/j.egyr.2022.04.047.

[24] D. Ginger, K. Fielding,The petroleum systems and future potential of the South Sumatra basin, In: Proceedings of the IPA 30th Annual Convention Proceedings, 2005. doi:10.29118/ipa.2226.05.g.039.

[25] T. Koning, N. Cameron, J. Clure, Undiscovered potential in the basement exploring in sumatra for oil and gas in naturally fractured and weathered basement reservoirs, Ber. Sediment. 47 (2) (2021) 67–79, https://doi.org/10.51835/bsed.2021.47.2.320.

[26] E. Sutriyono, E.W.D. Hastuti, B.K. Susilo, Geochemical assessment of late paleogene synrift source rocks in the south sumatra basin, Int. J. Geomate 11 (1) (2016) 2208–2215, https://doi.org/10.21660/2016.23.1141.

[27] T.F.K. Ngoroyemoto, J. Setyowiyoto, D.H. Barianto, Evaluating the implications of lineaments on petroleum fields: South sumatra, Indonesia, J. Appl. Geol. 6 (2) (2021) 77, https://doi.org/10.22146/jag.58161.

[28] S.K. Hansen, Y. Tao, S. Karra, Impacts of permeability heterogeneity and background flow on supercritical CO_2 dissolution in the deep subsurface, Water Resour. Res. 59 (11) (2023), https://doi.org/10.1029/2023WR035394.

[29] X.Y. Fang, Y.X. Lv, C. Yuan, et al., Effects of reservoir heterogeneity on CO_2 dissolution efficiency in randomly multilayered formations, Energies 16 (13) (2023), https://doi.org/10.3390/en16135219.

[30] H. Chen, B.R. Li, X.L. Liu, et al., CO_2 front migration law and injection-production optimization based on incomplete-miscible displacement, Energy Fuels 38 (19) (2024) 18888–18897, https://doi.org/10.1021/acs.energyfuels.4c03455.

[31] E.A. Al-Khdheeawi, S. Vialle, A. Barifcani, et al., Impact of reservoir wettability and heterogeneity on CO_2-plume migration and trapping capacity, Int. J. Greenh. Gas. Control 58 (2017) 142–158, https://doi.org/10.1016/j.ijggc.2017.01.012.

[32] H. Chen, X.L. Liu, C. Zhang, et al., Effects of miscible degree and pore scale on seepage characteristics of unconventional reservoirs fluids due to supercritical CO_2 injection, Energy 239 (2022) 122287, https://doi.org/10.1016/j.energy.2021.122287.

[33] H. Chen, C. Zhang, N. Jia, et al., A machine learning model for predicting the minimum miscibility pressure of CO_2 and crude oil system based on a support vector machine algorithm approach, no. December 2020, Fuel 290 (2021) 120048, https://doi.org/10.1016/j.fuel.2020.120048.

[34] M.G. Rezk, A.F. Ibrahim, Numerical investigation of CO_2 plume migration and trapping mechanisms in the sleipner field: Does the aquifer heterogeneity matter? (no. February), Fuel 394 (2025) 135054, https://doi.org/10.1016/j.fuel.2025.135054.

[35] Z. Rasheed, A. Raza, R. Gholami, et al., A numerical study to assess the effect of heterogeneity on CO_2 storage potential of saline aquifers, Energy Geosci. 1 (1–2) (2020) 20–27, https://doi.org/10.1016/j.engeos.2020.03.002.

[36] C. Harris, S.J. Jackson, G.P. Benham, et al., The impact of heterogeneity on the capillary trapping of CO_2 in the captain sandstone, Int. J. Greenh. Gas. Control 112 (2021) 103511, https://doi.org/10.1016/j.ijggc.2021.103511.

[37] S.J. Jackson, S. Krevor, Small-scale capillary heterogeneity linked to rapid plume migration during CO_2 storage, Geophys. Res. Lett. 47 (18) (2020), https://doi.org/10.1029/2020GL088616.

[38] E.A. Al-Khdheeawi, S. Vialle, A. Barifcani, et al., Effect of wettability heterogeneity and reservoir temperature on CO_2 storage efficiency in deep saline aquifers, no.

May 2017, Int. J. Greenh. Gas. Control 68 (2018) 216–229, https://doi.org/10.1016/j.ijggc.2017.11.016.
[39] N.I. Gershenzon, M. Soltanian, R.W. Ritzi, et al., Influence of small scale heterogeneity on CO_2 trapping processes in deep saline aquifers, Energy Procedia 59 (2014) 166–173, https://doi.org/10.1016/j.egypro.2014.10.363.
[40] E.M. Myshakin, F. Haeri, J. Moore, et al., Numerical simulations of carbon dioxide storage efficiency in heterogeneous reservoir models, Geofluids 2023 (2023), https://doi.org/10.1155/2023/5089508.
[41] K. Mawa, B.R.B. Fernandes, M. Delshad, et al., Assessing the influence of reservoir heterogeneity on CO_2 storage and dispersion patterns (no. July), Soc. Pet. Eng. SPE Conf. Oman Pet. Energy Show. OPES 2025 (2025), https://doi.org/10.2118/224835-MS (no. July).
[42] M.G. Bishop, South sumatra basin province, Indonesia: The Lahat/Talang Akar-Cenozoic total petroleum system, no. 99-50-S, USGS Open File Rep. (2001) 22.
[43] H. Doust, R.A. Noble, Petroleum systems of Indonesia, Mar. Pet. Geol. 25 (2) (2008) 103–129, https://doi.org/10.1016/j.marpetgeo.2007.05.007.
[44] W.A. Humairoh, H.D. Lakstianto, Analisis sedimentologi dan potensi reservoir pada formasi air benakat cekungan sumatra selatan, J. Ilm. Geol. Pangea 10 (2) (2023) 28–39.
[45] K. Idea, T. Marhaendrajana, I.G.B.E. Sucipta, et al., Rock mineralogy analysis of airbenakat formation to map the characteristics of the reservoir rocks in each depositional environment, J. Pet. Geotherm. Technol. 4 (2) (2023) 29–37.
[46] A. Haris, Integrated geological and geophysical approach to reservoir modeling: Case study of jambi Sub-basin, sumatra, Indonesia, J. Geol. Soc. India 95 (2) (2020) 197–204, https://doi.org/10.1007/s12594-020-1410-7.
[47] R. Setyawan, E.A. Subroto, B. Sapiie, et al., Geochemical and geomechanical study on gumai and talangakar formation to determine potential of shale gas in jambi Sub-Basin, south sumatra basin, J. Geosci. Eng. Environ. Technol. 5 (2) (2020) 94–102, https://doi.org/10.25299/jgeet.2020.5.2.4191.
[48] R. Rahadian, R. Winurani, C. Mustofa, et al., A Tight – Low Resistivity Coastal Deposit Reservoir as Potential Prospect in Sungai Gelam Area, jambi, IATMI, 2020.
[49] S. Tangparitkul, T. Akamine, R. Ramadhan, et al., CO_2 storage infrastructure and cost estimation for bioenergy with carbon capture and storage in Northern Thailand, Carbon Capture Sci. Technol. 15 (2025), https://doi.org/10.1016/j.ccst.2025.100425.
[50] R. Ramadhan, M. Abdurrahman, R. Bissen, et al., Numerical simulation of potential site for CO_2 sequestration in a depleted oil reservoir in Northern Thailand, no. S11, Energy Rep. 9 (2023) 524–528, https://doi.org/10.1016/j.egyr.2023.09.096.
[51] T. Ahmed, Fundamentals of Rock Properties, 5th ed. Gulf Publishing Company, 2019. doi: 10.1016/b978-0-12-813649-2.00004-9.
[52] J.R. Fanchi, "Porosity and Permeability," in Integrated Reservoir Asset Management, 2010, pp. 49–69. doi: 10.1016/b978-0-12-382088-4.00004-9.
[53] R. Wheaton, Basic Rock and Fluid Properties. 2016. doi: 10.1016/b978-0-08-101019-8.00002-8.
[54] D. Peng, D.B. Robinson, D. Peng, et al., A new two-constant equation of state a new two-constant equation of state, Ind. Eng. Chem. Fundam. 15 (1) (1976) 59–64.
[55] A.M. Rowe, J.C.S. Chou, Pressure-volume-temperature-concentration relation of aqueous NaCl solutions, J. Chem. Eng. Data 15 (1) (1970) 61–66, https://doi.org/10.1021/je60044a016.
[56] J. Kestin, H.E. Khalifa, R.J. Correia, Tables of the dynamic and kinematic viscosity of aqueous NaCl solutions in the temperature range 20 -150 °C and the pressure range 0.1–35 MPa, J. Phys. Chem. Ref. Data 10 (1981) 71–88, https://doi.org/10.1063/1.555641.
[57] L. Nghiem, V. Shrivastava, D. Tran, et al., "Simulation of CO_2 Storage in Saline Aquifers, SPE 125848," SPE/EAGE Reserv. Charact. Simul. Conf. held Abu Dhabi, UAE, no. July, pp. 1–15, 2009.
[58] L. Nghiem, V. Shrivastava, B. Kohse, et al., Simulation of trapping processes for CO_2 storage in saline aquifers, *CIPC 2009*, no. July, Can. Int. Pet. Conf. 2009 (2009), https://doi.org/10.2118/2009-156.
[59] M. Abdurrahman, A.K. Permadi, W.S. Bae, An improved method for estimating minimum miscibility pressure through condensation – extraction process under swelling tests, J. Pet. Sci. Eng. 131 (2015) 165–171, https://doi.org/10.1016/j.petrol.2015.04.033.
[60] N.I. Gershenzon, R.W.R. Jr, D.F. Dominic, et al., Water resources research, 2, JAWRA J. Am. Water Resour. Assoc. 5 (3) (1969) 2, https://doi.org/10.1111/j.1752-1688.1969.tb04897.x.
[61] M.A. Sohal, Y. Le Gallo, P. Audigane, et al., Effect of geological heterogeneities on reservoir storage capacity and migration of CO_2 plume in a deep saline fractured carbonate aquifer, Int. J. Greenh. Gas. Control 108 (2021), https://doi.org/10.1016/j.ijggc.2021.103306.

Romal is a PhD student at the Jackson School of Geosciences, The University of Texas at Austin. He received his BS and MS degrees in petroleum engineering and previously worked as a research associate at the Chiang Mai Research Center for Carbon Capture and Storage. His research focuses on subsurface fluid storage, induced seismicity and its associated geomechanical effects.

Muslim Abdurrahman is a professor of petroleum engineering at Universitas Islam Riau. He received his PhD in petroleum engineering from the Department of Energy and Mineral Resources at Sejong University. His research focuses on enhanced oil recovery, particularly CO_2 flooding.